Journal of Power Sources 196 (2011) 1184–1190

Contents lists available at ScienceDirect

Journal of Power Sources

journal homepage: www.elsevier.com/locate/jpowsour

Anode-supported microtubular cells fabricated with gadolinia-doped ceria nanopowders

V. Gil*, J. Gurauskis, R. Campana, R.I. Merino, A. Larrea, V.M. Orera

Instituto de Ciencia de Materiales de Aragón, C.S.I.C.-Universidad de Zaragoza, Pedro Cerbuna 12, E-50009 Zaragoza, Spain

ARTICLE INFO

Article history:
Received 16 April 2010
Received in revised form 16 August 2010
Accepted 30 August 2010
Available online 8 September 2010

Keywords:
Solid oxide fuel cell (SOFC)
Gadolinia-doped ceria (GDC)
Thin film electrolyte
Dispersion

ABSTRACT

Anode-supported microtubular SOFCs based on ceria 3 ± 0.2 mm diameter and about 100 mm in length have been prepared using gadolinia-doped ceria (GDC) nanopowders. Nanometric $Ce_{0.9}Gd_{0.1}O_{1.95}$ (GDC) powders were deposited on NiO–$Ce_{0.9}Gd_{0.1}O_{1.95}$ (NiO–GDC) anode supports by dip-coating technique. Fabrication conditions to obtain dense and gas tight electrolyte layers on porous microtubular supports were studied. Three different dispersing agents: commercial Beycostat C213 (CECA, France) and short chain monomer ($\leq$4 carbon atoms) with alcohol or carboxylic acid functional groups were evaluated. By optimizing colloidal dispersion parameters and sintering process, gas tight and dense GDC layers were obtained. Significantly lower sintering temperatures than reported previously ($\leq$1300 °C) were employed to reach $\geq$98% values of theoretical density within electrolyte layers of $\sim$10 μm in thickness. A composite cathode, LSCF–GDC 50 wt.% with about 50 μm thickness was dip coated on the co-fired half-cell and then sintered at 1050 °C for 1 h. The electrochemical performance of these cells has been tested. In spite of electronic conduction due to partial reduction of the thin-electrolyte layer, the *I–V* measurements show power densities of 66 mW cm^{-2} at 0.45 V at temperatures as low as 450 °C (using 100% H_2 as fuel in the anodic compartment and air in the cathodic chamber).

1. Introduction

Solid oxide fuel cell (SOFC) approach has been recognized as one of the most promising for converting chemical energy of fuel to electrical energy because of its high conversion efficiency, low emission of pollutants and useful fuel flexibility [1]. Furthermore, fuel versatility renders these devices suitable for portable devices fuelled with hydrogen, propane, diesel, etc. if the critical issues of the weight and long starting times could be solved. Portable applications for SOFC are envisaged in the fields of Auxiliary Power Units (APU) in transport, small power units for personnel, submarines, air planes, etc. Tubular design SOFCs were shown to be effective to realize such stacks since they possess high thermal shock resistance and they endure the thermal stress caused by rapid heating up to the operating temperature [2]. By decreasing the tubular cell diameter (microtubular SOFC with diameters in the millimetre range) it is expected to improve the mechanical behavior, thermal shock resistance as well as the volumetric power density of the cell stacks, due to the substantial increase in reactive area per unit volume. In addition, reduction of tube wall thickness significantly improves the mass transportation, which is one of the major barriers to the cell performance. Thus, it is crucial to develop fabrication technology of the microtubular SOFCs (with millimetre to submillimetre diameter) and their stacks.

Furthermore, more attention has been paid to solid oxide fuel cells operating at intermediate temperatures (500–700 °C, IT-SOFCs). In this temperature range, it is expected to decrease the material deterioration (that is to prolong the stack lifetime) and to reduce costs by incorporating metallic materials [3]. In order to reduce SOFC operating temperature there are two main strategies to follow: selection of appropriate electrolyte materials, with high ionic conductivity at low temperatures as for example, ceria based materials and/or to decrease the thickness of electrolyte to reduce the ohmic resistance losses.

Up to date, the most of the studies have been focused on the fabrication of yttria-stabilized zirconia (YSZ) microtubular cells, either based on the anode-supported thin-electrolyte [4,5] or on the electrolyte-supported design [6]. But only a few researchers have fabricated small-scale tubular SOFCs based on ceria [7–9]. For example, Liu et al. investigated cathode-supported microtubular SOFC (460 μm wall thickness and 2.26 mm in diameter) based on the cathode composition $La_{0.6}Sr_{0.4}Co_{0.2}Fe_{0.8}O_{3-\delta}$/$Ce_{0.9}Gd_{0.1}O_{1.95}$ (LSCF/gadolinia-doped ceria (GDC)) (60:40 volume). The maximum power densities for these cathode-supported cells were 160, 130

* Corresponding author. Current address: Department of Inorganic Chemistry, Norwegian University of Science and Technology (NTNU), 7034 Trondheim, Norway. Tel.: +47 73550878; fax: +47 73591105.
E-mail addresses: vanesa.hernandez@material.ntnu.no, vgil@unizar.es (V. Gil).

0378-7753/$ – see front matter © 2010 Elsevier B.V. All rights reserved.
doi:10.1016/j.jpowsour.2010.08.093

and 110 mW cm^{-2}, at 600, 550 and 500 °C, respectively for electrolyte thicknesses of *ca.* 12–15 μm. However the open circuit voltage (OCV) obtained here is relatively low if it is compared with the Nernst potential. The decrease being mainly related to the presence of internal short circuit current due to the mixed conductivity behavior of GDC electrolyte and the associated increase of electrode overpotentials. But also, the authors suggested that in LSCF supported GDC electrolyte extra losses may arise from the interfacial reaction associated with element diffusion from LSCF to GDC, which could cause degradation of the functional layer microstructures. Those chemical reactions produced an electrode polarization and in conclusion an electrode overpotential that drops the OCV.

The cathode-supported SOFCs present two disadvantages when compared with anode-supported ones. Firstly, in cathode-supported configuration the fuel is fed outside the tube, hence in the stack chamber. While in the anode-supported configuration the fuel flows up inside the microtubes. Secondly, the sintering temperature of the cathodes are usually lower than those typical for the anode materials and as a consequence it is more difficult to obtain tight electrolyte layers deposited on porous with these conditions.

Suzuki et al. [9] worked with anode-supported microtubular cells with 0.8–1.5 mm in diameter, reaching maximum power outputs up to 857 and 1017 mW cm^{-2} at 550 °C. In these designs the OCV values at 550 °C dropped from 0.96 to 0.83 when the thickness electrolyte was decreased down to 10 μm and the anode performance improved. The reason of the drop in OCV is again the reduction process of the ceria electrolyte, depending on the thickness as well as working temperature.

On the other hand, a critical problem of ceria-based electrolytes arises from the difficulty in GDC sintering near full density without formation of large grain sizes and in this way loosing mechanical strength. One way to improve sinterability and performance of GDC thin films is to use GDC nanopowders since the high surface area facilitates the sintering of ceramic bodies. However, very small grain size powders are prone to stimulate agglomeration during its deposition, which leads to grain coarsening and other detrimental effects during sintering. As a consequence, the right manipulation and optimization of GDC powder in colloidal suspensions is of critical importance for their successful utilization in ceramic processing. Up to now in order to sinter to suitable density the ceria based SOFC, sintering temperatures higher than 1350 °C and/or adding sintering additives are reported.

This research work aims to develop cell fabrication conditions from nanopowders to obtain dense $Ce_{0.9}Gd_{0.1}O_{1.95}$ (GDC) electrolyte layers (without using sintering additives) on porous microtubular supports (NiO–GDC) and to cosinter the half-cells at lower temperatures than state of art. After that, a not optimized cathode has been deposited and electrochemical testing of the cell has been carried out to elucidate which are the future improvement strategies.

As it was previously notice, several other researchers have reported, so far, the fabrication and testing of microtubular cells based on ceria, however the design or the concept were different, either cathode-supported or needle-type SOFCs and moreover, the sintering temperatures of the cells were above 1400 °C.

2. Experimental

The materials of the microtubular half-cells were chosen as follows: NiO–10% Gd-doped ceria (GDC–NiO 50 wt.%) as anode and 10% GDC as electrolyte. The procedure consists of the preparation of the anode tubes and the deposition of the electrolyte thin film followed by a co-sintering process. To optimize the co-sintering procedure the shrinkage of pellets of electrolyte and anode powders were measured by dilatometer (Setaram, SETSYS 2000, France) up to 1500 °C with a heating rate of 2 C min^{-1}.

Fabrication of the anode supports follows a similar procedure for fabrication of microtubular Ni/GDC cermets developed in a previous study [10]. The supports were processed using cold isostatic pressing from nanopowders 50 wt.% NiO/GDC (≤60 nm in size) synthesized by chemical route and with different characteristics, hence to control the final porosity of the support. Before the electrolyte thin film deposition, the green tubes were pre-sintered by heating up to 700 °C followed by a dwell time of 1 h.

Nanometric $Ce_{0.9}Gd_{0.1}O_{1.95}$ (GDC) powders (synthesized from the same method reported previously) were deposited on anode supports by colloidal processing route. A detailed study of the attrition milling conditions was carried out to eliminate the formation of large agglomerates of the nanopowders synthesized and to decrease their particle size in order to improve their sintering properties and densification behavior. Slurries for electrolyte dip coating (5 vol.% solids) were prepared by mixing the GDC powders, solvent (ethanol) and surfactants in attrition mill. Three different surfactant agents (3 wt.%); commercial Beycostat C213 (CECA, France) and two short chain monomers (≤4 carbon atoms) with alcohol and carboxylic acid functional group respectively (hereafter called R-OH and R′-COOH) were evaluated.

The agglomeration grade of the GDC powders and the particle size distribution (with and without surfactant) were studied by scanning electron microscopy (JEOL 6400) and by Laser Diffraction on a Malvern Nanosizer 2000 (Malvern, UK). More details comparing the type and quantity of dispersing agents and their effectiveness in different media is discussed along a future work [11].

Electrolyte deposition was performed using the best slurries conditions by dip coating with immersion and pulling out speeds within the range of 1–2 mm s^{-1}. The deposited electrolyte film was dried in air, and both anode and electrolyte were co-sintered in air at 1300 °C for 5 h. Scanning electron microscopy (JEOL 6400) was used to observe the thickness of the thin film electrolytes and their microstructures before and after the half-cell test. Overall, the half-cell preparation procedure involved simple ceramic processes based on two dip-coating depositions and just one sintering step.

The electrical performance of the half-cells was tested using a four-probe set-up at temperatures between 450 and 550 °C. Before that and in order to avoid damages in the electrolyte layer a 50 μm cathode functional layer (50 wt.% $La_{0.6}Sr_{0.4}Co_{0.2}Fe_{0.8}O_{3-\delta}$/$Ce_{0.9}Gd_{0.1}O_{1.95}$) was deposited by dip coating onto the co-sintered half-cell and later on sintered at 1050 °C for 1 h in air. The Ag wire was used for collecting current from anode and cathode, where the wire was fixed by using Pt paste. The final dimensions of the cells were an outside diameter of 3 ± 0.2 mm, wall thickness of 0.3 ± 0.03 and 90 mm in length. Current was collected in an effective area of 1 cm^2. Pure hydrogen 100 vol.% was used as fuel, flowed inside of the microtubular cell with a flow rate of 50 mL min^{-1} and the cathode side was open to the air. *I–V* curves were measured with a homemade electronic charge (Univ. Zaragoza, Spain).

3. Results and discussion

3.1. Powder properties

The microstructure of the GDC coatings strongly depends on the degree of the agglomeration between nanoparticles in the colloidal suspension. In order to obtain a fast sintering kinetics of these ceria based ceramics it is critical to keep grain agglomeration to a minimum, and as a consequence to achieve a high initial green density. Ceramic powders synthesized in this work presented primary par-

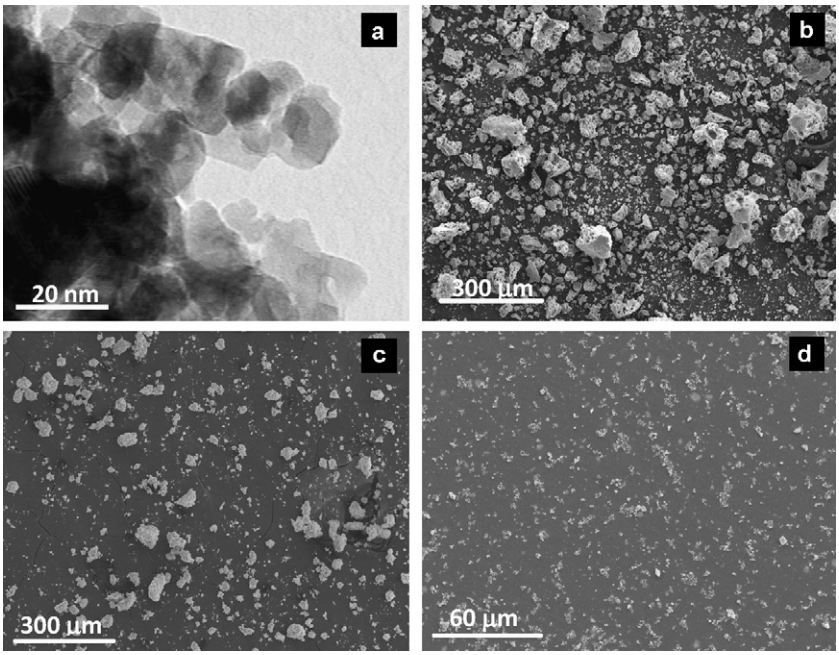

Fig. 1. GDC particle size: (a) TEM and (b) SEM micrographs of the as-synthesized and calcined powders, (c and d) SEM micrographs of the calcined powders after one and two milling cycles respectively.

ticle sizes under 20 nm. Fig. 1a shows a TEM micrograph of the starting GDC powders where it is possible to distinguish clearly the primary particle size. However, the calcined powders show a significant grain agglomeration by forming aggregates bigger than 150 μm (Fig. 1b). Attrition milling was used to eliminate these large agglomerates and to decrease the particle size. Best milling conditions consisted of milling cycles of 2 h duration at 1400 rpm in ethanol media. Fig. 1c shows that with the first milling cycle, just after the calcination process, the maximum size of the agglomerated particles decrease down 50 μm.

The presence of big agglomerates is reduced completely after two milling cycles leaving the maximum particle size down 1 μm (Fig. 1d). The milling procedure for the called "two milling cycles" should be run carefully just one cycle before and one cycle after calcination step. The characteristics of every cycle should be at 1400 rpm during 2 h. The reason of this surprising better milling procedure is due to the break of the big agglomerates just after they are formed during the synthesis procedure and before they become harder with the temperature of the calcining process.

In Fig. 2 is compared the particle size distribution of the powders after 1 or 2 milling cycles. From these measurements is corroborated that milling the powder before calcination process plays a key role decreasing agglomerate size.

So, the average agglomerate size is reduced from 4 μm to around 150 nm when one milling cycle before calcining process is applied. It should be noticed that in this case the particle size possesses a bimodal distribution with the major particles not only around 150 nm but also a small quantity around 500 nm exists.

Milling for longer times or cycles, does not improve the breaking of the agglomerates any further therefore the attrition was stopped after 2 cycles.

The influence of the attrition milling on the improvement of the densification behavior was studied by dilatometry measurements of GDC green compact pellets. The results of the dilatometry measurements are shown in Fig. 3. The significant variation in densification behavior between green compacts obtained from powders after either one or two milling cycles corroborates the importance of producing fine and non-agglomerated nanopowders. In fact, the powders obtained after two milling cycles could be packed down to densities ≥98% of the theoretical density at sintering temperature as low as 1350 °C and with only 2 h of dwell time as it is shown in Fig. 4 [12–14]. The excellent sintering behavior of our powders without the need of any sintering additives proves the effectiveness of the powder conditioning by the attrition milling procedure employed in this work.

In order to prevent the mechanical deterioration of the cell (cracking, delaminating or deformation) during the co-sintering process or in the cell operation, it is crucial to adjust the shrinkage behavior and achieve a good matching of thermal expansion coefficients (TEC) of cell components. As it was reported in a previous work both compositions NiO–GDC and GDC are thermomechanically compatible, i.e. the TECs values between them are closely matched ($\Delta\alpha = 0.8 \pm 0.1 \times 10^{-6}\,K^{-1}$) [10,15].

The shrinkage behavior during sintering of the two materials has been tailored by modifying the starting powder characteristics.

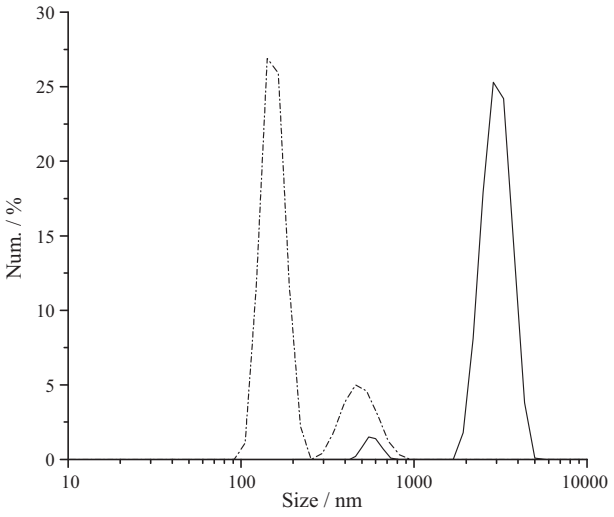

Fig. 2. Particle size distribution of GDC nanopowders in ethanol suspension after (—) one milling cycle and (- - - -) two milling cycles.

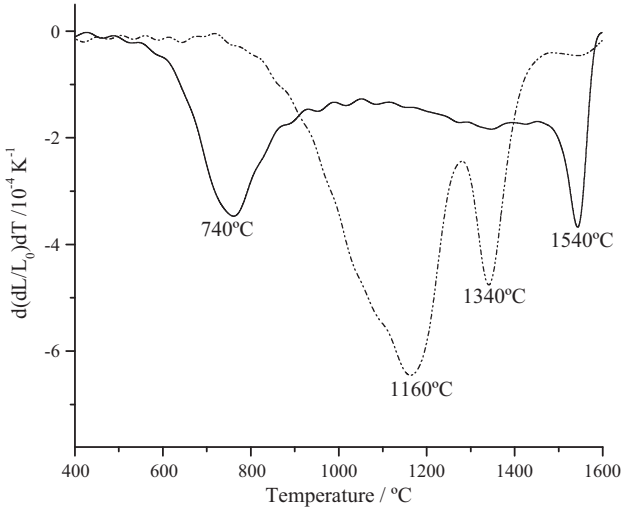

Fig. 3. Dilatometric curves for the GDC powders after one and two attrition milling cycles. (—) One milling cycle and (----) two milling cycles.

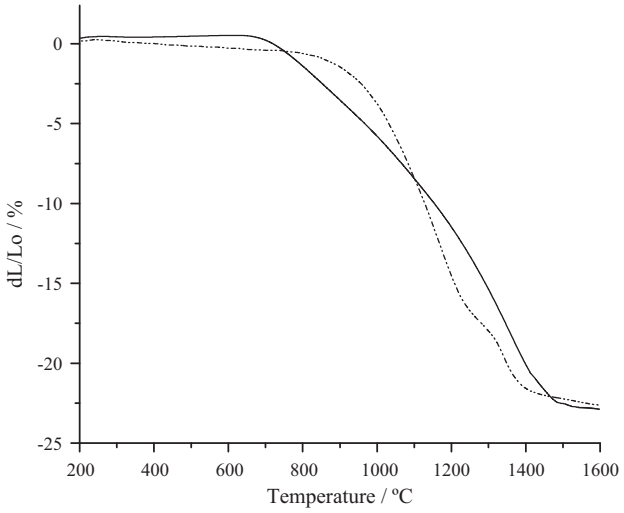

Fig. 5. Dilatometric curves during sintering of the anode and electrolyte powders, in air up to 1600 °C. (—) NiO–GDC anode support and (----) GDC electrolyte.

Although, it should be kept in mind that those dilatometry measurements were performed on powder pellets (Fig. 5) and not on deposited layers, these values are roughly approximate. It is clear that both anode and electrolyte powders achieve final shrinkages of ~22% when sintered to full density. In addition, pre-sintered substrate tubes (pre-sintered anode composition pellets) start to shrink at lower temperatures (700 °C vs. 800 °C) than the electrolyte materials which improves the densification of the electrolyte layers because of the induced compression stresses. Experiments carried out in air at 1300 °C for 5 h revealed than the densification kinetics and the final shrinkages of both the electrolyte and the anode are close and so the sintering of electrolyte layers at this low temperature was found to be sufficient to obtain good electrolyte tight layers as it is shown below.

3.2. Dip coating of electrolyte layers

As mentioned previously, good dispersion of the GDC nanopowders within the colloidal suspension is mandatory critical in order to obtain gas tight thin-electrolyte layer by dip-coating technique. To avoid agglomeration of GDC nanometric particles within the relatively concentrated solvent system (5 vol.% solids), the addition of 3 wt.% of different surfactants in ethanol media was studied.

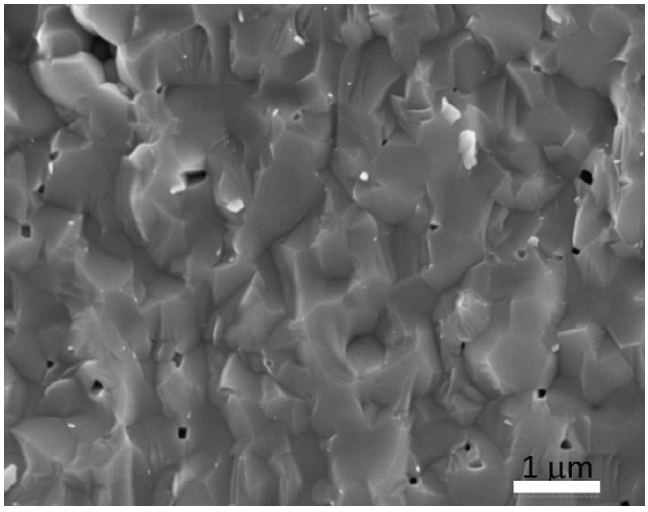

Fig. 4. Fracture SEM microstructure of a pellet sintered at 1350 °C for 2 h in air.

The particle size of the GDC nanoparticles dispersed within suspension is summarized in Fig. 6. With he commercial surfactant (Beycostat C213) the particle sizes present values above 5 µm. Submicronic sizes were obtained in the case of surfactant containing hydroxyl group (-OH) as the functional group. When a surfactant agent containing a terminal carboxylic acid (-COOH) was used (simple and short chain lengths with ≤4 carbon atoms), the mayor part of particles present in the suspension (Fig. 6) showed to be within nanometric range (<100 nm).

This proves that carboxyl radicals adsorbed on the particle surface results in effective steric hindrance stabilization mechanism between GDC nanoparticles thus preventing their agglomeration.

3.3. Microstructural characterization of anode-supported microtubular cell

In Fig. 7a and b the microstructure of GDC coatings on NiO–GDC substrates after being sintered at temperatures higher than 1350 °C is presented. The GDC coatings obtained with either a commercial Beycostat C213 or alcohol based dispersing agents showed a low final density even after sintering treatments above

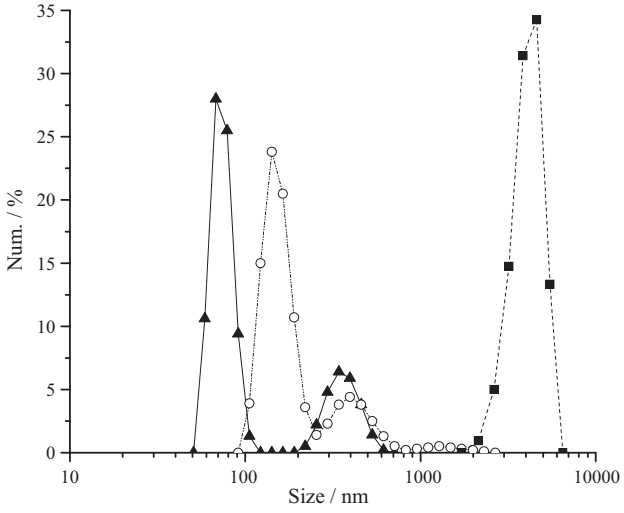

Fig. 6. Particle size distribution of GDC nanopowders in ethanol suspension when different surfactant agents are used: (▲) carboxylic acid (short chain), (◯) alcohol and (■) Beycostat C213.

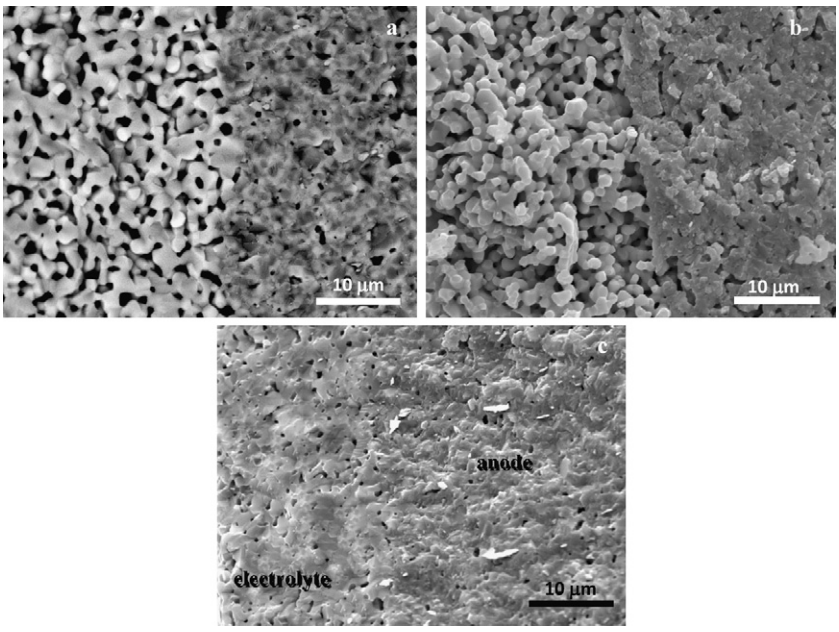

Fig. 7. Transverse cross-section SEM microstructures of GDC electrolyte (left side) dip coated onto NiO–GDC microtubular support. The darker phase (right hand side from images) corresponds to the NiO–GDC substrate and the brighter phase to the GDC coating. (a) Beycostat C213 as dispersing agent and half-cell co-sintered at 1400 °C for 2 h and (b and c) half-cells co-sintered at 1350 °C for 2 h with alcohol or carboxylic acid based dispersing agent, respectively.

1400 °C. Microstructural observations revealed the presence of high amounts of interconnected pores within the GDC layer thus leaving these coatings useless for electrolyte function. Since the densification mainly proceeds through grain boundary diffusion and in agreement with measurements of grain size distribution it is suggested that grain aggregation may slow down the ion mobility thus causing the observed decrease in densification. The effect of grain aggregation makes difficult the utilization of those nanocrystalline powders for tight layer fabrication.

The particle size distribution curves shown in Fig. 6 confirm that the nanopowder dispersion with an agent containing a terminal carboxylic acid should produce an improvement in the densification process. An example of thin film deposited by dip coating from a GDC slurry with this characteristics is shown in Fig. 7c. The transverse cross-sectional SEM micrograph of the half-cell is sintered at 1350 °C for 2 h and the 10–15 μm thick GDC layer presents nearly full density.

Concerning that, the electrolyte slurry choose to fabricate the SOFC was those with 3 wt.% of surfactant containing a terminal carboxylic acid and 3 or 4 carbon atoms in length.

Fig. 8a and b shows a transverse cross-section SEM micrograph of the cell co-sintered in two steps: first at 1300 °C for 5 h in air to cosinter anode and electrolyte and second at 1050 °C for 1 h in air in order to fire the functional cathode layer. The good adhesion between the layers of the pairs and the lack of structural defects (absence of cracks or delamination) confirms a good matching of the coefficients of thermal expansion during the sintering process.

The densification temperature in this work (≤1300 °C), is significantly lower than those reported previously for GDC [16]. This is mainly due to the optimized colloidal suspension where the major part of the particle size distribution stays below 100 nm. As a consequence of this, higher green densities and sintering kinetics of GDC nanopowders is obtained.

3.4. Electrochemical testing

Fig. 9 shows the *I–V* curves of the cell at 450 and 500 °C. As it is shown the cell polarization curves were almost linear in all the current density range studied. The measured open circuit voltages, OCV, were 0.78 and 0.74 at temperature 450 and 500 respectively.

Since a leak- and crack-free electrolyte layer could be assumed from SEM microstructures, this decreasing in the OCV values can be attributed to an internal short circuit current mainly related to the increasing electronic conductivity in ceria electrolyte due to reduction. Similar behavior of the OCV has been reported by other authors. Liu et al. [7] working in $La_{0.6}Sr_{0.4}Co_{0.2}Fe_{0.8}O_{3-\delta}$ cathode-supported $Ce_{0.9}Gd_{0.1}O_{1.95}$ thin-film found OCV values as low as 0.81 V at 450 °C operating temperature for a 50 mm thick elec-

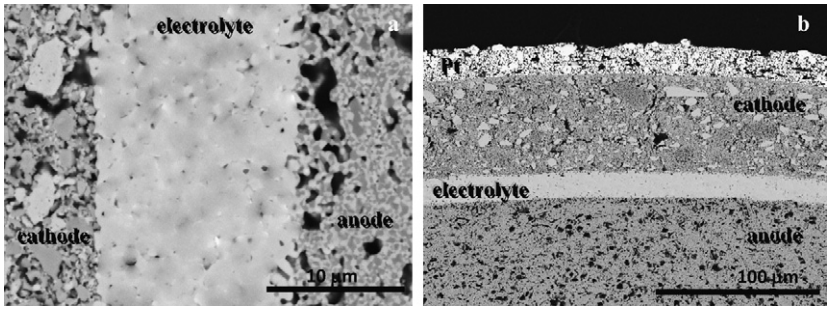

Fig. 8. Transverse cross-section SEM microstructure of anode-supported microtubular cell sintered at 1300 °C–5 h (a) cathode/electrolyte/anode and (b) Pt/cathode/electrolyte/anode.

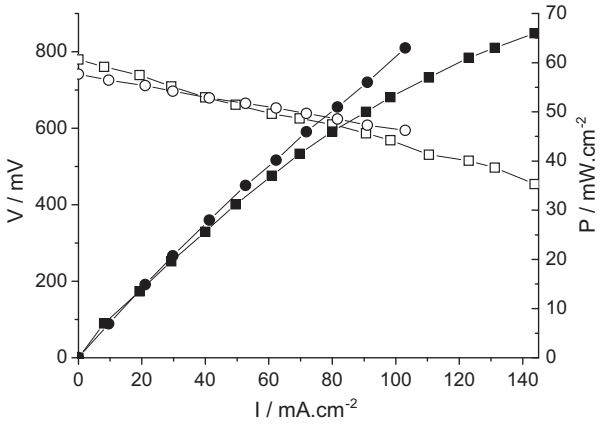

Fig. 9. Current–voltage (open symbols) and power density (closed symbols) characteristics of a co-fired anode-supported cell at (■, □) 450 °C and (●, ○) 500 °C.

trolyte. In addition, OCV voltage decreased to 0.75 V when the electrolyte thickness reduced to 20 μm. Suzuki et al. [9] worked with anode-supported needle-type micro SOFCs, the diameter of the needle-type cell is 0.4 mm and the GDC electrolyte thickness around 10 μm. For that geometry, the OCV dropped from 0.89 to 0.83 V as the operating temperature increased from 450 to 550 °C. However, the open circuit voltage increased up to 0.96 V when the thickness of the electrolyte increased to 30 μm and the anode was made less permeable for gasses. The same problem is also reported by Yamaguchi et al. [17] when working with anode-supported microtubular SOFC with 1.5 mm diameter, ~6 mm in length and thin film of 15 μm using a GDC electrolyte layer. In this case the open circuit voltages were below 0.90, 0.84 and 0.77 at 450, 500 and 550 °C, respectively.

In fact for doped ceria electrolytes, it is widely accepted the presence of considerable electronic conductivity as well as ionic conductivity under reducing conditions. Under operation conditions, one surface of the electrolyte material is exposed to the oxidizing atmosphere while the other surface to a strongly reducing atmosphere. If the electronic conduction of the electrolyte is not zero, the anode and cathode chambers are partly short-circuited by the electron flux through the electrolyte itself, leading to a loss of OCV [18] and even to water production in the fuel chamber in OCV conditions. We have indeed observed water formation at the exhaust of the tubes (anodic chamber) under zero current conditions.

In order to improve the OCV of the ceria based microtubular SOFCs, future developments on the cell structure and operation conditions will be required. In fact, increasing fuel humidification increases P_{O2} in the anodic chamber and decreases the reduction effect [19]. The optimization of the thickness of the electrolyte layer or/and the deposition of a second electrolyte layer, that is an electronic blocking layer [20,21] can also help to solve the problem. Wachsman [22] designed a bilayer electrolyte based on bismuth oxide/ceria in order to prevent the reduction of the ceria. An increase in the OCV of the bilayer electrolyte vs. the single ceria based electrolyte was obtained, however there were deviations from theoretical values. Between other reasons it is supposed the presence of cathodic polarization.

Riess et al. [23] reported the OCV values in SOFC are dependent not only on the thickness of the electrolyte but also on the overpotentials at the electrode/electrolyte interfaces related with the cell design and electrode microstructure. That is the internal shorting is not only dependent on the electronic conductivity of the GDC, but also on the kinetics of the oxygen reduction process. So, the electrode polarization due to non-reversible electrodes also contributes to the total cell voltage loss even at open circuit conditions, specially for cells based in thinner electrolytes, operating at lower temperatures and exposed to an atmosphere containing lower activity of electroactive species since electrode overpotential is a function of the ionic current density. Further Wang et al. [24] carried out simulation studies based on the local equilibrium steady state theory and they found that the main voltage drop comes from the electrolyte and the cathode polarization.

Although the cell seems to exhibit severe internal shorting attributed to the mixed conductivity of the thin GDC electrolyte, the power density obtained at 450 °C was as high as 66 mW cm^{-2} at 450 °C which is an encouraging result to further improve the cell output by increasing the electrolyte layer thickness and improving the quality of the cathode/electrolyte interface using these ceria nanopowders we have been able to prepare.

4. Conclusions

We succeeded in obtaining dense and tight GDC layers (≥98% dens. rel., ~10 μm thickness) co-fired on NiO–GDC anode supports at temperatures lower than those reported previously (≤1300 °C) and without the use of sintering aid additives. The fast sintering kinetics of our ceria based ceramics is a consequence of the careful control of the particle agglomeration state. The powders with the best dispersion properties (using R-OH or R-COH as surfactant agent) exhibit the lowest densification temperature. Particle agglomeration retarded the densification kinetics during the sintering process.

A laboratory-sized SOFC, with LSCF–GDC layer as the cathode, not yet optimized for performance, was shown to be feasible operating below 500 °C fed with pure H_2, and the maximum power density obtained at 450 °C was 60 mW cm^{-2} at 0.6 V.

The GDC layer obtained by this route presents a small grain size and a good electrochemical behavior which makes it suitable for electrolyte function in SOFC's. The relatively low-open circuit voltage obtained in the ceria based SOFC is probably due to the current leakage related to electronic conduction within the ceria electrolyte and the electrode overpotential, critical when using thin-electrolyte layers. Consequently, further developments are necessary to avoid the reduction of the electrolyte layer in order to maximize the efficiency of the cell.

Acknowledgments

This work was financed by the Spanish Government and the FEDER Program within the Projects: CEN 20071018, CIT-120000-2007-50 and MAT 2009-14324-C02-01.

References

[1] S.C. Singhal, K. Kendall, High Temperature Solid Oxide Fuel Cells: Fundamental, Design and Applications, Elsevier, Oxford, 2003.
[2] K. Kendall, M. Palin, J. Power Sources 71 (1998) 268.
[3] B.C.H. Steele, A. Heinzel, Nature 414 (2001) 345.
[4] Dhir, K. Kendall, J. Power Sources 181 (2008) 297.
[5] R. Campana, R.I. Merino, A. Larrea, I. Villarreal, V.M. Orera, J. Power Sources 192 (2009) 120.
[6] N.M. Sammes, Y. Du, J. Eur. Ceram. Soc. 21 (2001) 727.
[7] Y. Liu, S. Hashimoto, H. Nishino, K. Takei, M. Mori, J. Power Sources 164 (2007) 56.
[8] T. Suzuki, T. Yamaguchi, Y. Fujishiro, M. Awano, J. Power Sources 160 (2006) 73.
[9] T. Suzuki, Y. Funahashi, T. Yamaguchi, Y. Fujishiro, M. Awano, Solid State Ionics 180 (2009) 546.
[10] V. Gil, R. Campana, A. Larrea, R.I. Merino, V.M. Orera, Solid State Ionics 180 (2009) 784–787.
[11] V. Gil, J. Gurauskis, Study of doped-ceria nanopowders dispersing in suspension, paper under work.
[12] H. Yoshida, T. Inagaki, J. Alloys Compd. 408–412 (2006) 632.
[13] V. Gil, J. Tartaj, C. Moure, P. Durán, J. Eur. Ceram. Soc. 26 (2006) 3161.
[14] Q.L. Liu, S.H. Chan, C.J. Fu, G. Pasciak, Electrochem. Commun. 11 (2009) 871.
[15] V. Gil, J. Tartaj, C. Moure, Ceram. Int. 35 (2009) 839.

[16] T. Suzuki, Y. Funahashi, T. Yamaguchi, Y. Fujishiro, M. Awano, J. Power Sources 183 (2008) 544.
[17] T. Yamaguchi, T. Suzuki, S. Shimizu, Y. Fujishiro, M. Awano, J. Membr. Sci. 300 (2007) 45.
[18] T. Kawada, H. Yokokawa, Key Eng. Mater 125–126 (1997) 187.
[19] T. Matsui, M. Inaba, A. Mineshige, Z. Ogumi, Solid State Ionics 176 (2005) 647.
[20] S.H. Chan, X.J. Chen, K.A. Khor, Solid State Ionics 158 (2003) 29.
[21] D. Hirabayashi, A. Tomita, T. Hibino, M. Nagao, M. Sano, Electrochem. Solid-State Lett. 7 (2004) A318.
[22] E.D. Wachsman, Solid State Ionics 152–153 (2002) 657.
[23] I. Riess, M. Gödickemeier, L.J. Gauckler, Solid State Ionics 90 (1996) 91.
[24] S. Wang, T. Kato, S. Nagata, T. Kaneko, N. Iwashita, T. Honda, M. Dokiya, Solid State Ionics 152–253 (2002) 477.